Elevated IOP alters the space–time profiles in the center and surround of both ON and OFF RGCs in mouse

J. Sabharwal[a,b,c,1], R. L. Seilheimer[a,c], X. Tao[c], C. S. Cowan[c,2], B. J. Frankfort[b,c], and S. M. Wu[b,c]

[a]Medical Scientist Training Program, Baylor College of Medicine, Houston, TX 77030; [b]Department of Neuroscience, Baylor College of Medicine, Houston, TX 77030; and [c]Department of Ophthalmology, Baylor College of Medicine, Houston, TX 77030

Edited by John E. Dowling, Harvard University, Cambridge, MA, and approved July 10, 2017 (received for review May 1, 2017)

Glaucoma is a leading cause of blindness worldwide, and is characterized by progressive retinal ganglion cell (RGC) death. An experimental model of glaucoma has been established by elevating the intraocular pressure (IOP) via microbead occlusion of ocular fluid outflow in mice. Studies in this model have found visual dysfunction that varied with adaptational state, occurred before anatomical changes, and affected OFF RGCs more than ON RGCs. These results indicate subtle alterations in the underlying retinal circuitry that could help identify disease before irreversible RGC changes. Therefore, we looked at how RGC function was altered with elevated IOP under both photopic and scotopic conditions. We first found that responses to light offset are diminished with IOP elevation along with a concomitant decrease in receptive field center size for OFF RGCs. In addition, the antagonistic surround strength and size was reduced in ON RGCs. Furthermore, elevation of IOP significantly accelerated the photopic temporal tuning of RGC center responses in both ON and OFF RGCs. We found that some of the IOP-induced functional changes to OFF RGCs relied on ON cross-over pathways, indicating dysfunction in inner retinal circuitry. Overall, these results suggest that IOP alters multiple functions in the retina depending on the adaptational state. They provide a basis for designing multiple functional tests for early detection of glaucoma and for circuit-specific therapeutic targets in treatment of this blinding disease.

retinal ganglion cell | glaucoma | IOP | receptive field | multielectrode array

Glaucoma is one of the leading causes of blindness worldwide (1). It is a progressive disease and most patients are only identified after an irreversible visual deficit is already present (2). Diagnosing patients with subtle functional deficits that occur before this irreversible visual deficit will significantly improve a patient's ability to preserve normal vision.

Elevated intraocular pressure (IOP) is a critical risk factor for glaucoma and the central focus of glaucoma treatment (3, 4). Mouse models of glaucoma are also dependent on raising IOP. One method to elevate IOP is to inject microbeads into the eye to block normal fluid outflow (5). Previous studies on this mouse model have found that high IOP causes changes in retinal ganglion cell (RGC) anatomy and eventual cell death leading to irreversible vision loss as seen in glaucoma (5–7). Before these changes, functional properties, such as RGC light sensitivity and photopic receptive field (RF) center size, are altered (8–12). A better understanding of these functional changes may help to detect human disease before irreversible cell death.

In addition to RGC changes, behavioral tests have found that spatiotemporal tuning under photopic and scotopic conditions is altered (10). These behavioral studies suggest alteration in additional functional properties related to spatiotemporal tuning, such as scotopic receptive field size, temporal tuning, and the antagonistic surround.

To determine how these functions are altered, we used a multielectrode array (MEA) to record from a large population of RGCs and compare their functional properties in mice with and without bead-induced pressure elevation. We found that RGC responses were altered in the RF center for OFF RGCs and the RF surround for ON RGCs in bead-injected mice. Beyond RF spatial properties, temporal tuning was also accelerated. Finally, we showed that some of the IOP-induced changes to OFF RGCs are mediated by the ON cross-over circuitry.

Results

To study how elevated IOP alters retinal circuitry, we compared RGC functional properties in mice with and without bead injection. We performed MEA recordings on 12 control and 14 bead-injected retinas. RGC functional properties were determined by stimulating with both whole-field light steps and binary white-noise checkerboards at photopic and scotopic light levels.

RGC OFF Light Responses Are Reduced with IOP Elevation. To increase the IOP in mice, we used a variation of the microbead occlusion model (10–12). In all cases the left eye was injected with beads and the right eye was uninjected. Paired comparison of IOP from injected and uninjected eyes are shown in the graph in Fig. 1*A*.

We studied the whole-field response for each RGC by recording its response while alternating the screen from black to white at 4-s intervals. In Fig. 1*B* we show the average time-dependent firing rate across all cells ($n = 383$ control, $n = 306$ IOP). There was a significant reduction in the firing rate at light offset with IOP elevation ($P < 0.005$, rank-sum test), but not in the peak firing at light onset.

Significance

Glaucoma is a leading cause of blindness worldwide and many patients with glaucoma do not realize they have the disease until a significant visual deficit occurs. Here we record from mouse retinal ganglion cells and determine how they properties change in a mouse model of experiment glaucoma. We identify multiple changes to retinal ganglion cell functional properties and potential circuits mediating these changes. The findings from this study will help glaucoma patients in two ways. The novel functional changes we see can help identify new diagnostic tests that could identify patients prior to gross vision loss. Additionally, identification of specific retinal pathways mediating glaucomatous injury will help develop new treatments that extend to retinal cells that are currently being ignored.

Author contributions: J.S., B.J.F., and S.M.W. designed research; J.S., R.L.S., and X.T. performed research; J.S., C.S.C., B.J.F., and S.M.W. contributed new reagents/analytic tools; J.S. analyzed data; and J.S., R.L.S., X.T., C.S.C., B.J.F., and S.M.W. wrote the paper.

The authors declare no conflict of interest.

This article is a PNAS Direct Submission.

[1]To whom correspondence should be addressed. Email: jsab1208@gmail.com.

[2]Present address: Neural Circuit Laboratories, Friedrich Miescher Institute for Biomedical Research, 4058 Basel, Switzerland.

This article contains supporting information online at www.pnas.org/lookup/suppl/doi:10.1073/pnas.1706994114/-/DCSupplemental.

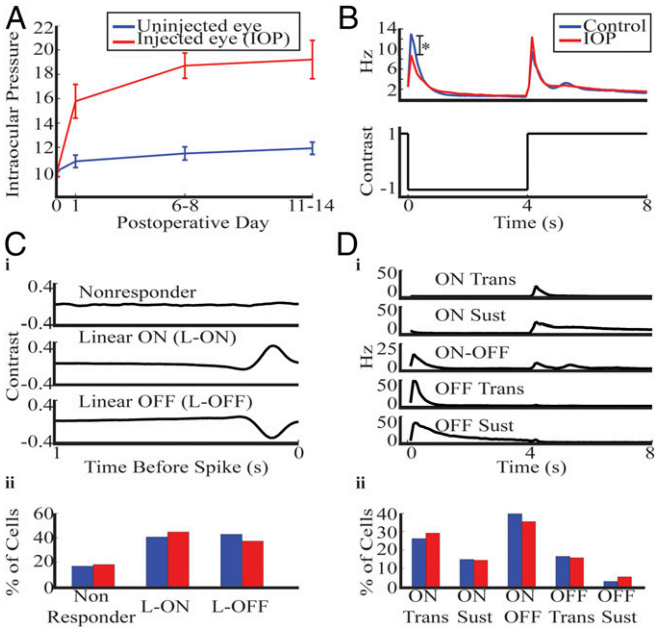

Fig. 1. Mice with bead injection had elevated IOP and reduction in OFF response. (*A*) Mean IOP from contralateral uninjected (blue) and injected (red) eye. Error bars show 1 SEM. (*B*) Whole-field time-dependent firing rate was averaged across the entire population of RGCs and plotted for control (blue) and IOP (red) mice. There was a significant reduction in OFF firing (*$P < 0.005$, rank sum). Control represents retinas from a separate population of mice that never received bead injection. (*C*, *i*) RGCs were divided into three groups based on their response to the white noise checkerboard. Average response in control retinas for each class are shown. (*ii*) The distribution of cells falling into each class is shown for control and IOP retinas. (*D*, *i*) RGCs were divided into five groups based on their response to the whole-field stimulus. Average response in control retinas for each class are shown. (*ii*) The distribution of cells falling into each class is shown. In addition, 20% of control, and 27% of IOP RGCs were unclassified by this system because either they did not respond to the whole field stimulus or they had a firing pattern diverging from the above classes.

To further study RGC properties, we compared their responses to the white-noise checkerboard stimulus (*Methods*). We computed a spike-triggered average (STA) on the same set of cells described above ($n = 419$ control, $n = 306$ IOP). In one control retina only the checkerboard stimuli were used, leading to a higher number of cells compared with the whole-field results. The total population was divided into cells that had a response to the checkerboard and those that did not (Fig. 1 *C*, *i*, row 1, Nonresponder). Cells were considered to have a response if any element of its STA exceeded 5 SD from its mean. Responsive RGCs were divided into linear ON and OFF classes based on the polarity of their peak response. The average peak temporal STA for each class is shown (Fig. 1 *C*, *i*, rows 2–3). There was no significant difference in class distribution with IOP elevation (Fig. 1 *C*, *ii*) ($P > 0.1$, χ^2). This linear ON and OFF (L-ON and L-OFF) classification will be used throughout the paper to compare functional properties.

The whole-field stimulus can also be used to divide the RGCs into five physiological classes (8, 13–15). In Fig. 1 *D*, *i* we show the average time-dependent firing rate for each class in control retinas. The response had the same shape in both conditions, but the ON-OFF and OFF transient cells had a significant reduction in firing rate at light offset with IOP elevation. The percentage of cells falling into each class was not significantly different between conditions (Fig. 1 *D*, *ii*) ($P > 0.1$, χ^2). The OFF sustained group will not be studied in the subsequent sections because too few cells had this response profile. The linear and physiological classification systems will help to identify which RGC subclasses mediated specific IOP-induced functional changes.

These results show that retinas from bead-injected eyes have elevated IOP and a decreased response to light offset. In addition, the distribution of cells falling into functional classes is unchanged from control mice, thus allowing us to compare properties of each RGC class. Because RGC whole-field responses were altered, we subsequently studied the effect of IOP elevation on the RGC linear space–time profile to identify additional functional alterations.

Spatial Processing in the Center and Surround Is Differentially Altered by IOP Elevation. Previous reports have shown that high IOP decreases photopic RF center size of RGCs, but its effect on the antagonistic surround and scotopic RFs was not studied (8, 9). Multiple circuits underlie the scotopic and photopic RF center and surround and they may be differentially susceptible to IOP (11). We therefore studied how IOP affects different components of RGC spatial processing.

We examined the antagonistic surround by dividing each cell's space–time STA into a center and surround region (Fig. 2*A*). The temporal traces within each were combined to form a single center and surround trace (Fig. 2*A*, black and green traces). To quantify surround strength, we use surround polarity index (SPI), the ratio of the area under the curve of the surround and center traces (*Methods*). In both control and bead-injected retinas, most cells had a negative SPI, indicating the antagonistic surround was still present with IOP elevation. Indeed, across the whole population there is no significant difference in SPI (Fig. 2 *B*, *i*). Subdividing based on the linear classification shows that L-ON cells have a nonsignificant increase in SPI, indicating a weaker antagonistic surround. The L-ON group includes ON Trans and Sust cells along with a subset of the ON-OFF cells. Interestingly only the ON Trans cells show an increase in their SPI (Fig. 2 *B*, *ii*). These results suggest that the circuitry driving the antagonistic surround of this subclass is more susceptible to IOP-induced changes.

To further study the circuitry mediating changes in the center-surround structure of RGCs, we determined the effect of IOP on the RF center and surround size. To do this we fit the space–time STA with the Sum of Separable Subfilters (SoSS) model, allowing us to identify the spatial properties of the center and surround (16).

We found that the average size of the RGC photopic RF center was significantly decreased across all RGCs with IOP elevation (Fig. 3 *A*, *i*). This effect was most pronounced in ON-OFF RGCs (Fig. 3 *A*, *ii*). For the photopic antagonistic surround size, we also saw a significant decrease across all RGCs (Fig. 3 *B*, *i*). In this case, the ON RGCs, especially ON Trans RGCs, showed

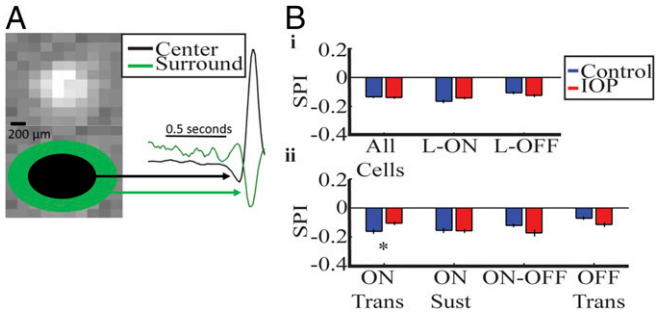

Fig. 2. Surround strength is decreased in ON transient RGCs and increased in OFF transient RGCs in IOP mice. (*A*) The spatial STA at the peak time for a sample cell is shown. Based on the spatial fit, a center region is defined from the center to 3 SD of the RF size (black ellipse). The surround region is defined from 3 SD to 9 SD (green ellipse). The black and green ellipses are shown for illustrations and are not to scale. On the *Right*, the traces within the center and surround region are combined to form a single trace for each region. The ratio of the surround to center quantifies the surround strength and is called SPI. (*B*, *i* and *ii*) SPI is compared for all RGC grouping, error bars represent 1 SE. The SPI is significantly weaker in ON Trans RGCs. *$P < 0.05$.

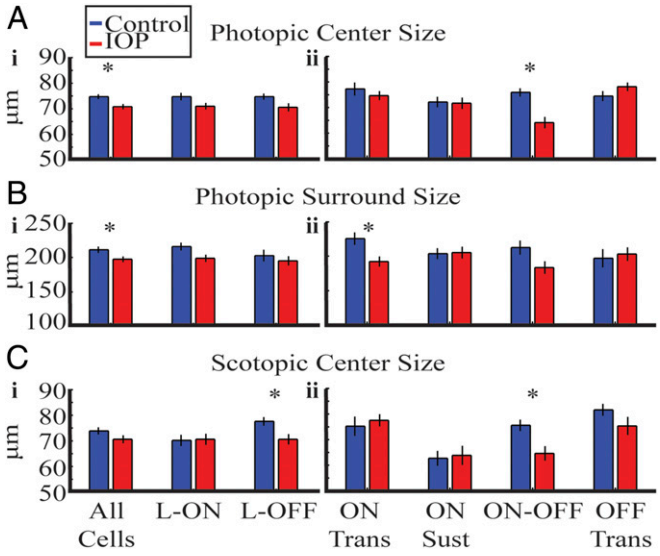

Fig. 3. The receptive field center-surround structure is altered by elevated IOP. (*A*) Photopic RF center size. (*i*) There is a significant decrease in the whole population and a trend toward significance for L-ON and L-OFF RGCs. (*ii*) ON-OFF RGCs show significant reduction. (*B*) Photopic RF surround size. (*i*) There is a significant decrease in whole population and a trend toward significance for L-ON RGCs. (*ii*) ON Trans RGCs show significant reduction. (*C*) Scotopic RF center size. (*i*) There is a significant decrease in l-OFF RF center size. (*ii*) ON-OFF RGCs show significant reduction. Error bars indicate 1 SEM. $*P < 0.05$.

the most profound change (Fig. 3 *B*, *ii*). These results show that the photopic center and surround sizes are differentially altered across RGC classes.

There was a significant decrease in scotopic RF center size for the L-OFF and ON-OFF RGCs (Fig. 3 *C*, *i* and *ii*). The antagonistic surround was not detectable for most cells under scotopic conditions for both groups so we could not compare them. Table 1 summarizes the spatial results outlined in this section. We did not observe a correlation between IOP elevation and RF change.

In summary, we showed that the RF center-surround spatial structure is altered with IOP, leading to an overall reduction in both components. This effect varied by RGC subclass and adaptation state. ON-OFF and OFF cells have smaller RF centers, whereas ON cells have a reduced surround strength and size. Multiple retinal circuits could be responsible for these functional changes. To better isolate the circuits damaged with IOP, we next studied the alteration in temporal properties of RGCs.

Temporal Tuning Is Accelerated in Mice with IOP Elevation. The temporal properties of RGCs are also dependent on the upstream retinal circuitry, but the effect of IOP on temporal properties has not been studied. In the previous section, we looked at the center and antagonistic surround by treating the center as a single component. We have previously shown that the temporal filter representing the RF center can be divided into three components forming a triphasic waveform (16) (Fig. 4 *A* and *B*). Each of these three components has distinct temporal properties that are quantified by their corner frequency. We compare the temporal properties of the three center and antagonistic surround components, hereafter referred to as center subfilters 1, 2, and 3 and surround subfilter 1.

First we confirmed that these subfilters are present in mice with elevated IOP under photopic and scotopic conditions. There is a significant acceleration of center subfilters 1 and 3 across all cells with IOP elevation under photopic conditions (Fig. 4*C*, *Upper*) ($P < 0.005$, rank sum). The temporal properties of subfilters are not significantly different under scotopic conditions (Fig. 4*C*, *Lower*). The corner frequency and SEM for each subfilter is shown in Table S1.

The alteration in center subfilter 3 is shown for each RGC class (Fig. 4*D*). The acceleration of center subfilter 3 is present in both L-ON and L-OFF RGCs and is primarily mediated by the ON and OFF Trans RGCs, respectively. Table 2 summarizes the temporal results.

In contrast to spatial alterations, temporal changes only occurred during photopic conditions. In addition, the temporal changes are observed for both ON and OFF RGCs. Center subfilters 1 and 3 both accelerate their temporal tuning, indicating an alteration in upstream circuits mediating low-frequency (slow) responses with IOP elevation. This indication is supported by the finding that center subfilter 3, the slow antagonistic component, is altered in more RGC classes (Table 2).

ON Cross-Over Circuits Contribute to IOP-Induced Alteration in OFF RGCs. We saw reduction in peak firing to whole-field stimuli and RF center size for OFF RGCs with IOP elevation. These alterations were also observed in OFF RGCs with the addition of the pharmacologic agent L-2-amino-4-phosphonobutyric acid (L-AP4), which blocks the photoreceptor to ON bipolar cell (BC) synapse (17). Blocking this synapse removes all ON pathways, which contribute to OFF RGCs via ON cross-over pathways. Recent work has suggested alteration of specific ON cross-over pathways with IOP elevation (11). Therefore, we wanted to test the hypothesis that some of the IOP-induced functional changes to OFF RGCs are mediated via ON cross-over pathways. We compared the previously published effects of L-AP4 on control retinas with the effect on retinas with elevated IOP. If the ON cross-over pathway is damaged in these retinas, the effect of L-AP4 should be reduced in magnitude or absent.

We previously looked at the effect of L-AP4 in control retinas ($n = 6$) and show the data here for comparison with retinas from mice with IOP ($n = 11$). Addition of L-AP4 resulted in loss of light responses from most L-ON RGCs but not L-OFF RGCs in control and IOP retinas. Therefore, we compared the effect of L-AP4 in L-OFF RGC functional properties from control ($n = 106$) and IOP ($n = 97$) RGCs.

We first looked at the peak firing rate of the OFF RGCs to the whole-field light step. The peak firing rate before L-AP4 was subtracted by the peak firing rate after L-AP4. The peak firing rate was decreased in both control and IOP retinas, but the magnitude of the difference was significantly smaller with IOP elevation (Fig. 5*A*, *Left* and Fig. S1) ($P < 0.005$, rank sum). Next, we similarly compared the L-AP4–induced alteration in RF center size. As with peak firing rate, L-AP4 caused a reduction in RF center size in both control and IOP retinas, but the magnitude was significantly smaller with IOP elevation (Fig. 5*A*, *Right* and Fig. S1) ($P < 0.005$, rank sum). The schematic in Fig. 5*B* summarizes these results.

Discussion

The primary goal of this paper was to determine how RGC responses change with IOP elevation and which retinal circuits could

Table 1. Spatial properties of the RGCs by group

RGC	SPI	Center size: Pho	Center size: Sco	Surr size
L-ON	—	—	—	—
L-OFF	—	—	▼	—
All	—	▼	—	▼
ON T	▼	—	—	▼
ON S	—	—	—	—
ON-OFF	—	▼	▼	—
OFF T	—	—	—	—

Surround size change is primarily mediated by ON Trans RGCs. Center size change is primarily mediated by L-OFF and ON-OFF RGCs. Arrowheads indicate significant decrease (Table S2).

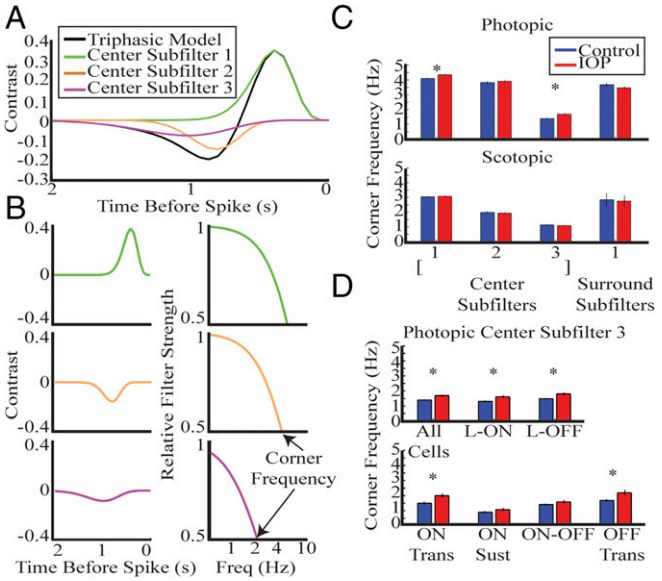

Fig. 4. RGCs accelerate temporal tuning in IOP mice. (*A*) Triphasic center trace is divided into three subcomponents. The three subcomponents are indicated by different colors and are referred to as center subfilters 1, 2, and 3. (*B*) Each subfilter is shown in a separate plot in the time domain in column 1, and in the frequency domain in column 2. The corner frequency can be identified for each cell by the frequency at which there is 50% attenuation. (*C*) The bar plot compares mean corner frequency for each subfilter in photopic (*Upper*) and scotopic (*Lower*) conditions. Error bar indicates 1 SE. (*D*) Mean corner frequency of center subfilter 3 is compared for each subclass. There is a significant increase for most classes. $*P < 0.05$.

underlie these changes. Elevation of IOP decreased RGC responses to light offset and reduced the RF center size in OFF RGCs. We also show that IOP elevation changes the antagonistic surround strength and size for ON RGCs. Furthermore, we found that IOP significantly accelerates temporal tuning of both ON and OFF RGCs. Taken together, these changes indicate an alteration in the upstream retinal circuitry. By comparing the effects of L-AP4 with IOP elevation, we identified a role of ON cross-over pathways in mediating IOP-induced functional changes to OFF RGCs.

Elevated IOP-Induced Changes to RGC Receptive Field Space–Time Structure. Multiple retinal circuits converge onto RGCs to help shape their functional properties, such as their light sensitivity (14, 18, 19) and center-surround structure (13, 20–22). We saw an IOP-induced decrease in firing rate in response to light offset for both OFF and ON-OFF RGCs. In addition, we also saw a decrease in L-OFF and ON-OFF RGC RF center size. The magnitude of this shift is similar to that seen by other investigators using similar methods (8). These changes could arise from IOP-induced alteration of the RGC dendrites in the OFF sublaminae (8, 23, 24). In addition to the RGC dendrites, other upstream retinal cell types, such as BCs or amacrine cells (ACs), are thought to mediate IOP-induced functional changes to RGCs (11). Our findings support this idea because we also find a reduction in the antagonistic surround strength and size in ON RGCs. The rod ON BC to AII AC synapse (RBC-AIIAC) is an example upstream retinal synapse that is altered with IOP elevation (11). This synapse could contribute to center responses of OFF RGCs (13, 20, 25) and surround responses of ON RGCs (26). In addition, the RBC-AIIAC circuit would contribute to RF center size under scotopic conditions (15), which we also show is reduced in L-OFF RGCs.

The SPI and surround size are distinct properties that can be independently altered with IOP. Interestingly, we found that the surround size was more sensitive to change with IOP than surround strength. This finding might suggest more distant surround inputs are selectively damaged. Alternatively, it may be possible that the dysfunction in the SPI with elevated IOP is compensated by another circuit component.

Temporal properties of RGCs are also dependent on these upstream circuits (20, 22), but the effect of IOP on temporal tuning has not been studied previously. We found that both ON and OFF RGCs accelerated their photopic temporal tuning. The average corner frequency for center subfilter 1 was 4.1 and 4.35 Hz for control and IOP animals, respectively (Table S1). Similarly, the average corner frequency of center subfilter 3 was 1.4 and 1.69 Hz, respectively. Under photopic conditions, both cone and mixed rod-cone circuits would be active for both ON and OFF RGCs (15, 18). RGC temporal tuning likely reflects the relative contribution of these different circuits. The RBC-AIIAC circuit is an example of a mixed rod-cone circuit and it would have slower temporal kinetics than cone circuits (15, 27). Weakening of the RBC-AIIAC synapse could increase the relative contribution of faster circuits, leading to an acceleration of the RGC temporal tuning. However, we also found that scotopic temporal tuning is not altered with IOP elevation. One explanation for this is that under scotopic conditions the RBC-AIIAC circuit is the primary driver of RGC responses (14, 19, 20). Weakening this synapse would not lead to a relative increase in contribution of faster circuits, therefore RGC response kinetics would not change.

Although the corner frequency shifts we show are small, they are comparable to changes seen with light adaptation (Table S1). This finding would indicate that IOP has a significant effect on visual processing at the RGC level, which could be measured at the behavioral level. Alteration in center-surround structure and corner frequency should lead to changes in the spatial and temporal contrast thresholds, respectively. Similarly, changing the whole-field firing should alter the contrast sensitivity. In fact, previous mouse studies have shown alteration in spatial and contrast thresholds with IOP (8, 10). Clinical tests already exist for features, such as spatial contrast sensitivity (28), and our results indicate temporal processing could be another feature susceptible to damage in ocular diseases. Furthermore, controlling the adaptation state of patients would also be important in these tests.

Upstream Circuits Mediating RGC Functional Changes. There has been a long history in connecting physiological changes in the retina with retinal cell types using electroretinograms (29, 30). Recent work has suggested that modeling RGC responses could provide insight into upstream circuitry (31, 32). Here, we also test the role of one of our purported circuits, the ON cross-over pathway, in underlying the RGC functional changes. Addition of L-AP4 removes all ON BC driven circuitry. Although ON BCs would be expected to drive ON and ON-OFF RGCs, they also contribute to OFF RGCs via ON cross-over pathways, as shown in Fig. 5*B* (25). L-AP4 completely abolishes light responses in L-ON RGCs, but only reduces the light response and RF center size of L-OFF RGCs in control retinas (20). These L-AP4–induced changes are decreased with IOP elevation, suggesting some of the IOP-induced changes rely on cross-over circuits.

Table 2. Temporal properties of the cells by group

Group	SF1	SF3
L-ON	▲	▲
L-OFF	-	▲
All	▲	▲
ON T	-	▲
ON S	-	-
ON-OFF	-	-
OFF T	-	▲

Center subfilter (SF1) is accelerated in IOP mice primarily in L-ON RGCs, whereas center subfilter 3 (SF3) is accelerated in both L-ON and L-OFF RGCs. The change in center subfilter 3 is mediated by ON and OFF Trans RGCs. Both ON Sust and ON-OFF RGCs had nonsignificant acceleration. Arrowheads indicate significant increase (Table S2).

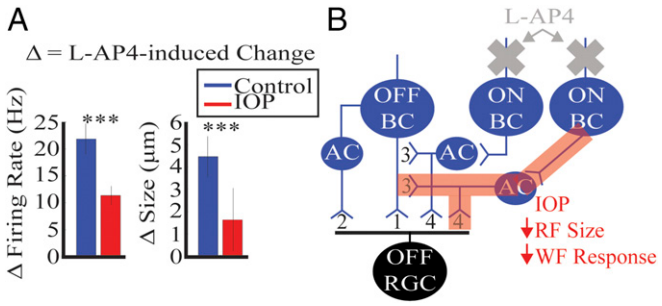

Fig. 5. ON cross-over circuits underlie some of the IOP-induced changes to OFF RGCs. (*A*) Peak firing rate to the whole field stimulus before L-AP4 is subtracted by the peak firing rate after L-AP4 and shown for both control (blue) and IOP (red) mice in the bar graph on the *Left*. The firing rate is decreased with L-AP4 in RGCs from both mice, but the decrease is significantly larger in control retinas. For photopic RF center size we only included RGCs that had good model fits before and after L-AP4 (control $n = 81$, IOP $n = 42$). RF center size before L-AP4 is subtracted by center size after L-AP4 and shown in the bar graph on the *Right*. The center size is similarly decreased for both control and IOP mice, but the decrease is significantly smaller in magnitude for IOP mice. Fig. S1 shows the baseline properties before and after L-AP4. Error bar indicates 1 SEM. ***$P < 0.005$. (*B*) Schematic illustrating pathways driving the OFF RGC and a model for IOP-induced damage. OFF BC driven circuits signal to OFF RGCs either directly (1) or indirectly (2) via AC. ON BC pathways can influence OFF RGCs through ACs either via feedback to OFF BCs (3) or feedforward to OFF RGCs (4). These are referred to as ON cross-over pathways (3, 4). Addition of L-AP4 removes all ON BC pathways (gray cross). Elevated IOP damages some ON BC pathways (red highlight) leading to decreased RF center size and whole response. Each pathway drawn encompasses multiple retinal circuits.

Thus, by combining inducible disease models with circuit dissection and functional testing, we identified a role for ON cross-over circuits in disease pathogenesis. Future studies can use other circuit dissection methods, including more specific pharmacologic agents or mutant mice, to hone in on specific susceptible retinal circuits.

Differential Effects of IOP on Various Physiological Types of RGCs. Work from multiple laboratories has indicated that high IOP causes selective anatomic changes to OFF sublaminae in the inner plexiform layer and dysfunction in OFF RGCs (8, 23, 24). Consistent with this, we found reduction in light offset-induced spiking in OFF and ON-OFF RGCs. Our finding is also consistent with reduction in RF center size for OFF RGCs (8, 9). In addition, because we extended our functional analysis to include whole-field response, antagonistic surround, and temporal processing, we found significant changes in ON RGC responses. These results support the idea that IOP has effects across the entire inner plexiform layer and perhaps beyond the direct synapse between BCs and RGCs (11). Here we determined a role for the ON cross-over pathways that could help explain the fact that we see functional changes in both ON and OFF RGCs. These findings suggest a significant role for studying the effect of IOP on retinal circuitry alongside RGC subtypes.

Some of the class-specific IOP-induced changes we found differ significantly from results in recent papers (33). For example, we find that the RF center size of OFF transient RGCs is unchanged, ON-OFF RGCs are decreased, and the RF sizes were previously found to be reduced and unchanged, respectively (8, 9, 24). Consistent with our findings, anatomical studies have found subclasses of ON-OFF RGCs have altered dendritic processes with IOP (23). The differences we see in our functional results could arise from differential experimental conditions. For example, our IOP was less elevated, our experiments were performed under more dark-adapted conditions, and our photopic light level was dimmer than that used in other studies. We also showed that some IOP-induced changes differed under scotopic and photopic conditions (temporal tuning) (Fig. 4). Together, these observations identify multiple IOP-induced dysfunctions present under different conditions (level of IOP and adaptation state), and provides basis for designing multiple functional tests for early detection of glaucoma in the clinic. Determining the anatomic components underlying these different functional changes would also provide an avenue to circuit-specific therapy in the treatment of glaucoma (34, 35).

Methods

Ethical Approval. Mice (C57BL/6J from Jackson laboratories) were cared for following approved protocols from the Animal Care and Use Committee of Baylor College of Medicine and in compliance with the National Institutes of Health guidelines for the care and use of experimental animals.

IOP was elevated in the left eye by performing bead injections on 10-wk-old mice 13–16 d before physiological experiments. Bead injections were performed after intraperitoneal injection of anesthetic (mixture of ketamine, xylazine, and acepromazine). The details of this procedure have been outlined previously (10–12). Eye pressure in control and injected eyes were checked with a TonoLab rodent tonometer (36).

MEA Recording. Mice were kept on a regular light/dark cycle and experiments were performed diurnally. Mice were dark-adapted for at least 60 min before being killed. Killing was performed by cervical dislocation while under a surgical plane of anesthesia. Retinal electrophysiology was carried out as indicated in our previous publications (14, 16). In brief, eyes were removed under infrared illumination using night vision scopes (Nitemare; BE Meyers) and whole-mount retinas were placed onto a MEA, ganglion cell side down. Recordings were made primarily from the central retina. The MEA-60 (Multichannel Systems) had 60 electrodes spaced 100 μm apart, each with a diameter of 10 μm. RGC action potentials were recorded at 20 KHz and prefiltered with a 0.1-Hz high-pass hardware filter.

The retina was kept at 35.6 °C and perfused with carboxygenated (95% O_2, 5% CO_2) recording solution (NaCl 124 mM, KCl 2.5 mM, $CaCl_2$ 2 mM, $MgCl_2$ 2 mM, NaH_2PO_4 1.25 mM, $NaHCO_3$ 26 mM, and glucose 22 mM at pH 7.35) (37). Some experiments were performed with standard recording solution only. Other experiments had standard recording solutions for the first half and were then perfused with 20 μM L-AP4 mixed into the solution (20). MEA recordings lasted about 4 h per retina. Standard single-unit identification procedures were performed to identify activity of distinct units across the entire recording session (38). Experimental preparation (axotomy, flat mount, and so forth) does cause acute pressure change on retinas. The control group serves to normalize this effect but the acute changes may mask or enhance the effect of IOP because of beads.

Stimulation. Similar to our previous report (16) and those of others (39), the ambient white light level during an experiment was measured as wavelength-specific irradiance [E(λ), in microwatts cm^{-2}] in the plane of the preparation (S170C; Thor Labs and SpectraRad; Edmund Optics). The mean ambient photopic light level was 140 R* per rod per second. Neutral density filters were used to create three log unit attenuation, creating an ambient scotopic light level of 0.14 R* per rod per second. Stimuli were projected as an optically reduced image from a computer monitor which presented light from the visible spectrum (SXGA-JF311-5100; Dell). A beam splitter was used to present the image from the computer monitor from below the MEA.

Whole-Field Light Stimulation. Classic physiological classes were identified by a stimulus protocol consisting of 30 repeated trials of 4 s of a black screen followed by 4 s of a white screen. ON/OFF/ON-OFF was determined as described in other reports (8, 14). Transient and sustained classification was determined by manual selection (*SI Methods* and Fig. S2).

White-Noise Receptive Field Mapping. Receptive fields were mapped using random binary white-noise checkerboards presented at 15 Hz. Each square in the checkerboard was either black or white and 50 μm on a side. The stimulus was created and presented with PsychToolbox (40, 41). Reverse correlation was used to compute a space–time spike-triggered average (STA) (42, 43). Given the 15-Hz stimulation, we were limited to responses up to 7.5 Hz. Based on the corner frequencies of our temporal filters and previous studies carried out under similar light levels, the RGC responses should fall well below this (44). Cells were identified as linear ON or OFF (referred as L-ON and L-OFF in *Results*) based on the peak response of their STA.

Spatial Pooling and Surround Characterization. The STA was first fit to the product of a spatial Gaussian and the impulse response of a temporal filter (45). The spatial Gaussian determines the size of the 1-σ distance in the major and minor axis. This was used to determine identify 1-σ annular zones. Temporal traces within zones 1–3 were combined to form a single center trace, and those in zones 4–9 were combined to form a surround trace. By summing the first 150 ms of the center and surround trace we identified a single value to characterize the center and surround. The ratio of these values (surround/center) was calculated and is reported here as the SPI (16). A negative value indicates opposite polarity of the center and surround. A larger number indicates a stronger surround.

The SoSS Model. The SoSS model is described in our previous report (16), but briefly it models the receptive field as the sum of up to five subfilters. Each subfilter has a unique temporal and spatial filter. The temporal filter function is shown in Eq. **1** (46), and the spatial filter was a standard 2D Gaussian (16, 45). The product of these generates the space–time response for each subfilter *i*.

$$f_i(t) = p_i(t/\tau_i)^{n_i-1}\left(e^{-t/\tau_i}\right)\Big/\tau_i(n_i-1)! \qquad [1]$$

The temporal properties (τ_i and n_i) along with the scale (p_i) were independent for each subfilter. All subfilters for a single cell had the same 2D spatial Gaussian (center location and orientation), but its spatial extent could vary. We compared the annular-averaged raw data with annular-averages fit data with a weighted least-squares regression. The weights were the square root of the number of spatial inputs in each annulus. For each cell an *F*-test was used for model comparison with determine how many subfilters were needed.

Center and Surround Size. Center subfilter 1's 1-σ spatial extent can be used to describe the RF center size, whereas that of surround subfilter 1 can be used for the RF surround size. The 1-σ spatial extent has a major and minor axis and the geometric mean of the two were used to identify the RF size in this paper.

Statistical Tests. Unless otherwise indicated, *t* tests were used for statistical testing and significance was determined by $P < 0.05$. Bonferroni correction was applied when multiple comparisons were made by subdividing RGCs (Table S2). When data were not normally distributed ,Wilcoxon signed-rank test or rank sum (Mann–Whitney *U*) test was used for paired or unpaired comparisons, respectively.

ACKNOWLEDGMENTS. This work was supported by NIH Grants EY019908 (to S.M.W.), EY025601 (to B.J.F.), EY025480 (to J.S.), and EY002520 (to S.M.W.), as well as the Retina Research Foundation (S.M.W. and B.J.F.), and an unrestricted grant from Research to Prevent Blindness to Baylor College of Medicine.

1. Quigley HA, Broman AT (2006) The number of people with glaucoma worldwide in 2010 and 2020. *Br J Ophthalmol* 90:262–267.
2. Weinreb RN, Khaw PT (2004) Primary open-angle glaucoma. *Lancet* 363:1711–1720.
3. Kass MA, et al. (2002) The Ocular Hypertension Treatment Study: A randomized trial determines that topical ocular hypotensive medication delays or prevents the onset of primary open-angle glaucoma. *Arch Ophthalmol* 120:701–713; discussion 829–830.
4. Leske MC, et al.; Early Manifest Glaucoma Trial Group (2003) Factors for glaucoma progression and the effect of treatment: The early manifest glaucoma trial. *Arch Ophthalmol* 121:48–56.
5. Sappington RM, Carlson BJ, Crish SD, Calkins DJ (2010) The microbead occlusion model: A paradigm for induced ocular hypertension in rats and mice. *Invest Ophthalmol Vis Sci* 51:207–216.
6. Chen H, et al. (2011) Optic neuropathy due to microbead-induced elevated intraocular pressure in the mouse. *Invest Ophthalmol Vis Sci* 52:36–44.
7. Cone FE, Gelman SE, Son JL, Pease ME, Quigley HA (2010) Differential susceptibility to experimental glaucoma among 3 mouse strains using bead and viscoelastic injection. *Exp Eye Res* 91:415–424.
8. Della Santina L, Inman DM, Lupien CB, Horner PJ, Wong RO (2013) Differential progression of structural and functional alterations in distinct retinal ganglion cell types in a mouse model of glaucoma. *J Neurosci* 33:17444–17457.
9. Chen H, et al. (2015) Progressive degeneration of retinal and superior collicular functions in mice with sustained ocular hypertension. *Invest Ophthalmol Vis Sci* 56: 1971–1984.
10. van der Heijden ME, et al. (2016) Effects of chronic and acute intraocular pressure elevation on scotopic and photopic contrast sensitivity in mice. *Invest Ophthalmol Vis Sci* 57:3077–3087.
11. Pang JJ, Frankfort BJ, Gross RL, Wu SM (2015) Elevated intraocular pressure decreases response sensitivity of inner retinal neurons in experimental glaucoma mice. *Proc Natl Acad Sci USA* 112:2593–2598.
12. Frankfort BJ, et al. (2013) Elevated intraocular pressure causes inner retinal dysfunction before cell loss in a mouse model of experimental glaucoma. *Invest Ophthalmol Vis Sci* 54:762–770.
13. van Wyk M, Wässle H, Taylor WR (2009) Receptive field properties of ON- and OFF-ganglion cells in the mouse retina. *Vis Neurosci* 26:297–308.
14. Cowan CS, et al. (2016) Connexin 36 and rod bipolar cell independent rod pathways drive retinal ganglion cells and optokinetic reflexes. *Vision Res* 119:99–109.
15. Pang JJ, Gao F, Wu SM (2004) Light-evoked current responses in rod bipolar cells, cone depolarizing bipolar cells and AII amacrine cells in dark-adapted mouse retina. *J Physiol* 558:897–912.
16. Cowan CS, Sabharwal J, Wu SM (2016) Space-time codependence of retinal ganglion cells can be explained by novel and separable components of their receptive fields. *Physiol Rep* 4:e12952.
17. Slaughter MM, Miller RF (1981) 2-amino-4-phosphonobutyric acid: A new pharmacological tool for retina research. *Science* 211:182–185.
18. Wu SM, Gao F, Pang JJ (2004) Synaptic circuitry mediating light-evoked signals in dark-adapted mouse retina. *Vision Res* 44:3277–3288.
19. Völgyi B, Deans MR, Paul DL, Bloomfield SA (2004) Convergence and segregation of the multiple rod pathways in mammalian retina. *J Neurosci* 24:11182–11192.
20. Sabharwal J, Seilheimer RL, Cowan CS, Wu SM (2016) The ON crossover circuitry shapes spatiotemporal profile in the center and surround of mouse OFF retinal ganglion cells. *Front Neural Circuits* 10:106.
21. Dedek K, et al. (2008) Ganglion cell adaptability: Does the coupling of horizontal cells play a role? *PLoS One* 3:e1714.
22. Pandarinath C, et al. (2010) A novel mechanism for switching a neural system from one state to another. *Front Comput Neurosci* 4:2.
23. El-Danaf RN, Huberman AD (2015) Characteristic patterns of dendritic remodeling in early-stage glaucoma: Evidence from genetically identified retinal ganglion cell types. *J Neurosci* 35:2329–2343.
24. Ou Y, Jo RE, Ullian EM, Wong RO, Della Santina L (2016) Selective vulnerability of specific retinal ganglion cell types and synapses after transient ocular hypertension. *J Neurosci* 36:9240–9252.
25. Werblin FS (2010) Six different roles for crossover inhibition in the retina: Correcting the nonlinearities of synaptic transmission. *Vis Neurosci* 27:1–8.
26. Bloomfield SA, Xin D (2000) Surround inhibition of mammalian AII amacrine cells is generated in the proximal retina. *J Physiol* 523:771–783.
27. Ke JB, et al. (2014) Adaptation to background light enables contrast coding at rod bipolar cell synapses. *Neuron* 81:388–401.
28. Dorr M, Lesmes LA, Lu ZL, Bex PJ (2013) Rapid and reliable assessment of the contrast sensitivity function on an iPad. *Invest Ophthalmol Vis Sci* 54:7266–7273.
29. Brown KT (1969) The electroretinogram: Its components and their origins. *UCLA Forum Med Sci* 8:319–378.
30. Abd-El-Barr MM, et al. (2009) Genetic dissection of rod and cone pathways in the dark-adapted mouse retina. *J Neurophysiol* 102:1945–1955.
31. Real E, Asari H, Gollisch T, Meister M (2017) Neural circuit inference from function to structure. *Curr Biol* 27:189–198.
32. Cowan CS, Sabharwal J, Seilheimer RL, Wu SM (2017) Distinct subcomponents of mouse retinal ganglion cell receptive fields are differentially altered by light adaptation. *Vision Res* 131:96–105.
33. Della Santina L, Ou Y (2017) Who's lost first? Susceptibility of retinal ganglion cell types in experimental glaucoma. *Exp Eye Res* 158:43–50.
34. Weitlauf C, et al. (2014) Short-term increases in transient receptor potential vanilloid-1 mediate stress-induced enhancement of neuronal excitation. *J Neurosci* 34: 15369–15381.
35. Akopian A, Kumar S, Ramakrishnan H, Viswanathan S, Bloomfield SA (2016) Amacrine cells coupled to ganglion cells via gap junctions are highly vulnerable in glaucomatous mouse retinas. *J Comp Neurol*, 10.1002/cne.24074.
36. Pease ME, Cone FE, Gelman S, Son JL, Quigley HA (2011) Calibration of the TonoLab tonometer in mice with spontaneous or experimental glaucoma. *Invest Ophthalmol Vis Sci* 52:858–864.
37. Tian N, Copenhagen DR (2003) Visual stimulation is required for refinement of ON and OFF pathways in postnatal retina. *Neuron* 39:85–96.
38. Anishchenko A, et al. (2010) Receptive field mosaics of retinal ganglion cells are established without visual experience. *J Neurophysiol* 103:1856–1864.
39. Sinclair JR, Jacobs AL, Nirenberg S (2004) Selective ablation of a class of amacrine cells alters spatial processing in the retina. *J Neurosci* 24:1459–1467.
40. Brainard DH (1997) The psychophysics toolbox. *Spat Vis* 10:433–436.
41. Pelli DG (1997) The VideoToolbox software for visual psychophysics: Transforming numbers into movies. *Spat Vis* 10:437–442.
42. Meister M, Pine J, Baylor DA (1994) Multi-neuronal signals from the retina: Acquisition and analysis. *J Neurosci Methods* 51:95–106.
43. Chichilnisky EJ (2001) A simple white noise analysis of neuronal light responses. *Network* 12:199–213.
44. Pandarinath C, Victor JD, Nirenberg S (2010) Symmetry breakdown in the ON and OFF pathways of the retina at night: Functional implications. *J Neurosci* 30:10006–10014.
45. Chichilnisky EJ, Kalmar RS (2002) Functional asymmetries in ON and OFF ganglion cells of primate retina. *J Neurosci* 22:2737–2747, and erratum (2002) 22:1a.
46. Watson AB (1986) Temporal sensitivity. *Handbook of Perception and Human Performance* (Wiley, New York).